PCCP

ROYAL SOCIETY OF CHEMISTRY

PAPER

View Article Online
View Journal | View Issue

Cite this: *Phys. Chem. Chem. Phys.*, 2025, **27**, 8932

Microwave spectroscopy of the vinylperoxy radical, CH_2CHOO†

Masakazu Nakajima [a] and Yasuki Endo [b]

Received 18th February 2025,
Accepted 22nd March 2025

DOI: 10.1039/d5cp00649j

rsc.li/pccp

Vinylperoxy radicals were produced in a pulsed supersonic jet by discharging a gas mixture of vinyl bromide and molecular oxygen largely diluted in the Ar or Ne buffer gas. Two conformers of the radical, s-*trans* and s-*cis*, were detected through their pure rotational transitions *via* Fourier-transform microwave spectroscopy. Fine and hyperfine components in the observed spectra were fully assigned and analyzed to determine precise molecular constants for each conformer. The Fermi coupling constants determined for the $-CH_2$ protons indicate that non-negligible unpaired spin density is located on the terminal carbon atom, although the radical is generally considered as the oxygen-centered radical. The intensities of the observed spectra are much weaker than expected, probably because most of nascent vinylperoxy radicals formed by the association of the vinyl radical and O_2 promptly dissociate either to the vinoxy radical and atomic oxygen, or to formaldehyde and the formyl radical, even under jet-cooled conditions.

1. Introduction

The vinyl radical (C_2H_3) is one of the simplest hydrocarbon radicals with unsaturated C–C bonds. The reaction of the radical with molecular oxygen is thought to play important roles in hydrocarbon oxidation, and its importance is often mentioned and demonstrated through combustion models of ethylene.[1–5] Experimental kinetic studies on the reaction have thus been reported by many research groups,[6–13] and the temperature- and pressure-dependences of the overall rate constant are well characterized. Because of high exothermicity of the reaction, many exothermic product channels may compete with each other. Knowledge on energetically accessible product channels and the product branching ratio is thus essential for characterizing this important reaction. Several theoretical studies exploring the potential energy surface of $C_2H_3 + O_2$ have so far been reported,[2,13–18] and many exothermic product channels together with their reaction mechanisms have been proposed. From theoretical analyses on the product branching ratio[1,2,13,15,16,18–21] and experimental detections of the products,[6,7,11–13,17,22–24] the vinoxy radical (CH_2CHO) + O channel and the formaldehyde (HCHO) + formyl radical (HCO) channel are generally accepted to be predominant in the $C_2H_3 + O_2$ reaction. Theoretical analyses on product-specific rate coefficients[1,2,13,15,16,18–21] show that the CH_2CHO + O channel is more important at higher temperature, and the formation of HCHO is predominant at lower temperature. Because of the high exothermicity of the HCHO + HCO channel, the product HCO may further dissociate to H + CO.

$$C_2H_3 + O_2 \rightarrow (C_2H_3OO)^* \rightarrow CH_2CHO + O$$
$$\rightarrow HCHO + HCO$$
$$\rightarrow \text{other product channels.}$$

The first step of the $C_2H_3 + O_2$ reaction is bimolecular association, yielding the vinylperoxy radical (VPR; C_2H_3OO). Nascent VPRs are highly excited because of the high exothermicity of the reaction, so that they promptly dissociate to CH_2CHO + O, or undergo intramolecular isomerization to the three-membered ring form $^{\bullet}CH_2$-*c*-C(H)OO (dioxiranyl-methyl), finally leading to the HCHO + HCO dissociation. Some of the nascent VPRs are expected to be collisionally stabilized under high-pressure conditions, and the stabilized radicals may be extinguished by reactions with other molecules.

As briefly mentioned above, many experimental and theoretical studies on the $C_2H_3 + O_2$ reaction have been reported because of its importance in hydrocarbon oxidation. However, knowledge on the intermediate, VPR, is quite limited. So far, several spectroscopic studies have been reported for this radical through its vibrational and electronic transitions. UV-visible spectra of the radical have been observed in aqueous solutions[25,26] and in the gas-phase.[24,27] The observed spectra show a structureless broad absorption in the range of 220–500 nm with a strong feature centered at about 250 nm. In the gas-phase experiments,[24,27] the vinyl radical generated by

[a] *Department of Basic Science, The University of Tokyo, 3-8-1 Komaba, Meguro-ku, Tokyo 153-8902, Japan. E-mail: nakajima@bunshi.c.u-tokyo.ac.jp*
[b] *Department of Applied Chemistry, National Yang Ming Chiao Tung University, 1001 Ta-Hsueh Rd., Hsinchu 300093, Taiwan. E-mail: endo@nycu.edu.tw*

† Electronic supplementary information (ESI) available: Theoretical equilibrium geometries, vibration–rotation constants, and frequency lists of observed microwave transitions for the *s-trans*- and *s-cis*-vinylperoxy radicals. See DOI: https://doi.org/10.1039/d5cp00649j

photolysis of ether vinyl bromide (C_2H_3Br) or methyl vinyl ketone ($CH_3COC_2H_3$) was converted to the VPR by the association with O_2, and the transient absorption was observed. On the other hand, the reported transient absorption was absent in a similar gas-phase experiment with a lower concentration of the vinyl radical.[13] The spectral carrier of the reported UV-visible gas-phase spectra[24,27] seems to be still open for discussion. An infrared spectrum of the VPR was reported using the matrix-isolation technique by Yang *et al.*[17] They prepared the radical by the $C_2H_3 + O_2$ reaction in an Ar matrix, and two absorption features at 1140.7 and 875.5 cm^{-1} were identified to be attributed to the VPR, with the help of density functional calculations and isotope substitution experiments. As far as the author's knowledge, only a preliminary observation has been reported for the near-IR absorption of the gas-phase VPR by the Miller group.[28] They have systematically observed near-IR cavity-ringdown absorption spectra for many alkylperoxy radicals prepared by the alkyl radical association with O_2 in the gas phase.[29] The preliminary observation provided highly congested spectra in which the carrier species is strongly inferred to be the VPR. However, the identification of the spectral carrier is still tentative.[28]

In this paper, we report Fourier-transform microwave spectra of two conformers (s-*trans* and s-*cis*) of the VPR generated by the reaction $C_2H_3 + O_2$. Because the radical is an open-shell species and has three protons with a nuclear spin of 1/2, its rotational spectrum splits into a number of fine and hyperfine components. We observed microwave spectra showing such congested structures, and the spectral carrier was unambiguously identified to be the VPR by fully analyzing the observed fine and hyperfine components. Precise molecular constants were determined for each of the conformers by least-squares analysis for a data set of the observed line frequencies. At the end of this article, we will make a brief discussion on the product branching of the reaction $C_2H_3 + O_2$, based on the spectral intensities of the VPR, the vinoxy radical, and formaldehyde, observed in the same discharged jet.

2. Quantum chemical calculation

Prior to a spectral survey of the VPR, quantum chemical calculations were carried out to predict its rotational transition frequencies and spectral splitting patterns due to the unpaired electron and the nuclear spins of protons. The MOLPRO software package[30] was used for molecular geometry optimizations based on the coupled cluster method, and Gaussian 16[31] was used for predictions of the fine/hyperfine coupling constants and molecular anharmonic properties with density functional theory.

As shown in Fig. 1, the VPR has two stable conformers depending on the direction of the O–O bond relative to the C–C bond.[16,17,21,27,32] Both of them are planar with C_s symmetry, and one conformer with the O–O bond located at the *trans* position is referred to as s-*trans*-VPR, and the other is s-*cis*-VPR. Molecular geometry of each conformer was optimized by referring to the electronic energy calculated at the RCCSD(T)-F12a level of theory using the cc-pCVTZ-F12 basis set, with all the core electrons included in the electron correlation as well as the valence electrons. The optimized bond lengths and angles of each conformer are given in Fig. S1 of the ESI.† The optimized geometries show reasonable agreements with those previously reported.[15–18,27,32] Zero-point energy correction on the electronic energy at the optimized geometry was made by calculating harmonic vibrational frequencies at the B3LYP/aug-cc-pVTZ level of theory. The zero-vibrational level of the s-*trans*-VPR was predicted to be lower in energy by 312 cm^{-1} than that of the s-*cis*-VPR. Zero-point vibrational corrections on the equilibrium rotational constants corresponding to the optimized geometry of each conformer were made by using the vibration–rotation α constants calculated at the B3LYP/aug-cc-pVTZ level of theory. The theoretical harmonic frequencies and the vibration–rotation constants used for the zero-vibrational correction are listed in Table S1 of the ESI.† The theoretical energy difference between the two conformers and the predicted rotational constants are summarized in Table 1.

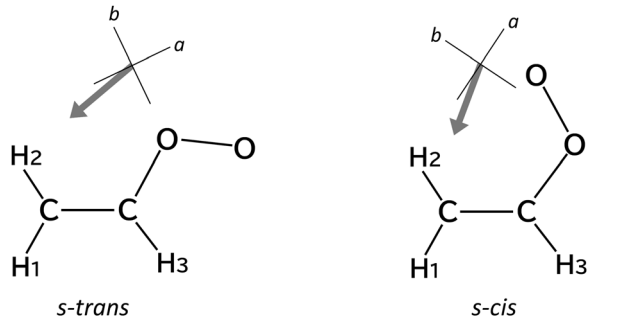

Fig. 1 Two conformers of the vinylperoxy radical. The s-*cis*-conformer is predicted to be higher in energy than the s-*trans*-conformer by 312 cm^{-1} (*cf.* Table 1). The direction of the theoretically calculated permanent dipole moment is shown for each conformer as a bold gray arrow together with the principal *a*- and *b*-axes.

Table 1 Theoretically predicted energy difference, rotational constants, and dipole moment components of the vinylperoxy radical at the RCCSD(T)-F12a/cc-pCVTZ-F12 level of theory (all the core electrons are included in the electron correlation)

	s-*trans*	s-*cis*
ΔE_e/cm^{-1}	0	284
A_e/MHz	51 118	21 441
B_e/MHz	4964	7009
C_e/MHz	4525	5282
ΔE_0[a]/cm^{-1}	0	312
A_0[b]/MHz	50 602	21 367
B_0[b]/MHz	4934	6946
C_0[b]/MHz	4497	5239
$\lvert\mu_a\rvert$/D	2.44	2.28
$\lvert\mu_b\rvert$/D	0.65	0.60

[a] Zero-point energy is estimated from theoretical harmonic frequencies calculated at the B3LYP/aug-cc-pVTZ level of theory. [b] Zero-vibrational corrections are made using theoretical vibration–rotation constant α calculated at the B3LYP/aug-cc-pVTZ level of theory.

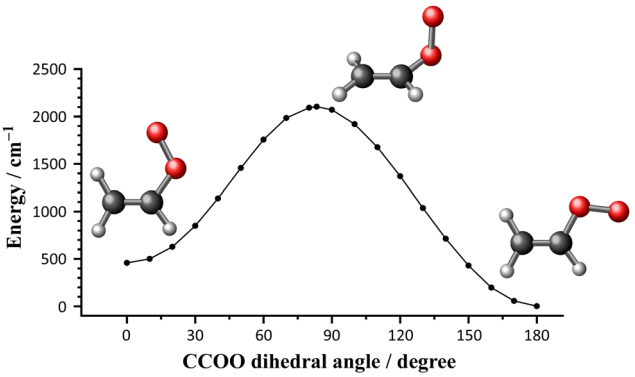

Fig. 2 Potential energy curve of the vinylperoxy radical along the CCOO dihedral angle. The electronic energy is calculated at the B3LYP/aug-cc-pVTZ level of theory with all the geometrical parameters other than the CCOO dihedral angle relaxed. The transition state is located at an angle of 83.3°.

The components of the permanent dipole moment along the principal axes were obtained for each conformer by computing the electronic energies at the same level of theory as the geometry optimization, with an external electric field virtually applied along the principal axes. The results are listed in Table 1. The direction of the dipole moment (see Fig. 1) is almost parallel to the principal *a*-axis of each conformer. Fine and hyperfine coupling constants of each conformer were also predicted by using the NMR properties keyword of Gaussian 16 program at the B3LYP/aug-cc-pVTZ level of theory.

The minimum energy path of the interconversion between the two conformers is thought to be along the coordinate of the CCOO dihedral angle. Fig. 2 shows the B3LYP/aug-cc-pVTZ potential energy curve calculated by changing the dihedral angle from 0° (s-*cis*) to 180° (s-*trans*) with other geometrical parameters fully relaxed. The interconversion barrier is estimated to be roughly 2000 cm^{-1}, which is in good agreement with the previously estimated values.[21,28]

3. Experimental

The VPR was produced in a pulsed-supersonic jet by an electric discharge of a gas mixture containing precursor molecules. Typically, a gas mixture, 0.3% of vinyl bromide, 2% of O_2, and *ca.* 98% of the buffer gas (either Ne or Ar), was prepared. The premixed gas of 2–3 atm was expanded into a vacuum chamber using a pulsed solenoid valve, and a pulsed voltage of 1.2 kV was applied between electrodes attached at the nozzle exit of the valve, synchronized with the valve opening.[33] The association reaction of the discharge product C_2H_3 with O_2 may yield both the s-*trans*- and s-*cis*-conformers of the VPR in the present experiment. As seen in Fig. 2, there exists a high energy barrier (*ca.* 2000 cm^{-1}) for the interconversion between the two conformers, so that the nascent production ratio may be "frozen" in the supersonic jet, and both of the conformers are expected to be observed.

A Balle–Flygare type Fourier-transform microwave (FTMW) spectrometer[34] operated in the frequency region of 4–40 GHz was used for the observation of microwave transitions. In order to reduce the Doppler broadening of spectral lines, the discharged jet expanded into the cavity of the spectrometer coaxially with the microwave propagating axis, although two Doppler components appeared in the spectrum for each MW transition.[35] The rotational temperature of molecules in the jet was thought to be less than 3 K. The Earth's magnetic field in the center region of the MW cavity was cancelled out by using three Helmholtz coils to prevent spectral line splitting due to the Zeeman effect.

An FTMW-MW double-resonance technique[36] was employed for observing several weak b-type transitions of the VPR. In the double-resonance experiment, a certain microwave transition was monitored with an FTMW spectrometer, and then the frequency of the pump MW radiation, which illuminated the discharged jet after the irradiation of the probe MW pulse for FTMW spectroscopy, was scanned. In this case, the macroscopic polarization induced by the probe MW pulse is "broken" if the pump MW is resonant with a transition of which either the upper or lower level is shared by the monitored transition, so that depletion of the monitored signal is observed as the double-resonance signal.

4. Results and analysis

According to the theoretical dipole moments listed in Table 1, the intensities of b-type rotational transitions of the VPR are expected to be much weaker than those of a-type transitions. Furthermore, for the s-*trans*-conformer, the frequencies of b-type transitions, of which lower rotational levels are located at sufficiently low energy for moderate thermal population under jet-cooled conditions, are out of the operation frequency range of our FTMW spectrometer (4–40 GHz). Thus, only a-type transitions of both conformers were surveyed by FTMW spectroscopy. The spectral splitting pattern of each rotational transition of the VPR was simulated with the theoretically predicted fine/hyperfine constants, prior to the spectral survey. Microwave transitions of paramagnetic species showing similar splitting patterns to the simulations were then surveyed. As a result, five a-type transitions with $K_a = 0$ or 1, 1_{01}–0_{00}, 2_{02}–1_{01}, 3_{03}–2_{02}, 2_{12}–1_{11}, and 2_{11}–1_{10}, were observed for the s-*trans*-VPR. In addition, one b-type transition, 1_{11}–2_{02} at around 46 GHz, was observed with the double-resonance technique by monitoring individual fine/hyperfine components of the 2_{02}–1_{01} transition. A total of 81 paramagnetic lines including well separated fine and hyperfine components were observed for the s-*trans*-VPR. All of them are listed in Table S2 of the ESI.† Quantum numbers labeling each observed line are defined by the coupling scheme, $\mathbf{J} = \mathbf{N} + \mathbf{S}$, $\mathbf{F}_1 = \mathbf{J} + \mathbf{I}(H_1)$, $\mathbf{F}_2 = \mathbf{F}_1 + \mathbf{I}(H_2)$, and $\mathbf{F} = \mathbf{F}_2 + \mathbf{I}(H_3)$, where $\mathbf{N}$ and $\mathbf{S}$ are the rotational and electron spin angular momenta, respectively, $\mathbf{I}$ is the nuclear spin angular momentum of each proton, and $\mathbf{F}$ is the total angular momentum. Note that only the total angular momentum $\mathbf{F}$ is the good quantum number, and $\mathbf{J}$ is a nearly good quantum number for labeling the electron spin component. However, the intermediate quantum numbers, $\mathbf{F}_1$ and $\mathbf{F}_2$, have little importance in physics.

A reduced form of the spin-rotation Hamiltonian[37] for doublet asymmetric top molecules of C_s symmetry, together

with the hyperfine interaction Hamiltonian due to the three protons of the VPR, was used to reproduce the energy levels of the radical. A least-squares analysis of the experimental frequency data was carried out with a homemade program. A somewhat detailed description of the analysis program and comparisons with the spfit/spcat program suite,[38,39] which is an analysis tool widely used for high-resolution spectroscopy, has been given elsewhere.[40] Molecular constants determined for the s-*trans*-VPR are listed in Table 2 together with the theoretically predicted constants. Twenty-one parameters are determined from the 81 line positions, and all the observed line positions are reproduced with the standard deviation of 3.1 kHz, comparable to the expected experimental accuracy ~ 3 kHz. The determined molecular constants show reasonable agreements with the theoretical ones, being strong evidence for the identification of the spectral carrier.

For the s-*cis*-VPR, four a-type transitions, 1_{01}–0_{00}, 2_{02}–1_{01}, 2_{12}–1_{11}, and 2_{11}–1_{10}, were observed by FTMW spectroscopy, and one b-type transition 1_{11}–0_{00} was observed with the double-resonance technique by monitoring the 1_{01}–0_{00} transition. The intensities of the observed FTMW spectra were about one-half to one-third of those of the s-*trans*-VPR, probably reflecting the energy difference between the two conformers. A total of 48 lines including fine and hyperfine components were observed for the s-*cis*-VPR (*cf.* Table S3 of the ESI†), and 18 molecular parameters were determined by a least-squares analysis, as listed in Table 2. The standard deviation of the fit is 6.0 kHz, which is slightly larger than the expected experimental accuracy. A larger error may be introduced in reading line positions from the s-*cis* VPR spectra, because they were generally weak and observed with poor S/N ratios.

Table 2 Molecular constants of the vinylperoxy radical in the ground vibronic state (in MHz)

	s-*trans*-conformer		s-*cis*-conformer	
	Experiment[a]	Theory[b]	Experiment[a]	Theory[b]
A	50 491.8388(34)	50 602	21 225.108(10)	21 367
B	4925.66940(57)	4934	6951.4084(11)	6946
C	4490.74247(63)	4497	5235.4680(11)	5239
$10^3\Delta_N$	1.161(21)	1.10	5.03[c]	5.03
$10^3\Delta_{NK}$	−7.03(36)	−5.47	−18.32(60)	−20.0
$10^3\Delta_K$	507[c]	507	80.9[c]	80.9
$10^3\delta_N$	0.121[c]	0.121	1.55[c]	1.55
$10^3\delta_K$	6.30[c]	6.30	10.2[c]	10.2
ε_{aa}	−2970.6129(62)	−2292.3	−616.078(12)	−494.4
ε_{bb}	−88.3943(44)	−76.0	−374.8321(93)	−285.2
ε_{cc}	−1.0690(38)	2.7	−0.8914(90)	3.3
$(\varepsilon_{ab} + \varepsilon_{ba})/2$	−163.78(13)	−363.7	294.768(80)	274.3
a_F (H_1)	−10.4117(39)	−11.194	−10.063(13)	−10.770
T_{aa} (H_1)	2.5423(48)	2.733	6.810(21)	8.429
T_{bb} (H_1)	−2.002(15)	−2.233	−6.084(46)	−7.603
T_{ab} (H_1)	−5.49(34)	−6.674	−1.472[c]	−1.472
a_F (H_2)	−8.6212(46)	−9.695	−10.007(14)	−10.856
T_{aa} (H_2)	−0.6959(79)	−2.372	2.362(17)	1.136
T_{bb} (H_2)	2.459(16)	4.140	1.007(33)	1.881
T_{ab} (H_2)	3.51(37)	2.971	1.22(42)	−0.132
a_F (H_3)	2.9815(31)	3.252	1.1987(64)	2.644
T_{aa} (H_3)	4.5530(47)	5.249	5.420(11)	5.983
T_{bb} (H_3)	0.818(18)	0.283	−1.380(28)	−1.714
T_{ab} (H_3)	−6.73(33)	−7.319	−2.712[c]	−2.712

[a] Values in parentheses are 1σ error and applied to the last digits. [b] Rotational constants are cited from Table 1. Centrifugal distortion constants and spin coupling constants are predicted using Gaussian 16 software suite,[31] by computing vibrational–rotational coupling (VibRot keyword), and NMR shielding tensors and magnetic susceptibilities (NMR keyword), respectively, at the B3LYP/aug-cc-pVTZ level of theory. [c] Fixed.

5. Discussion

A planar equilibrium geometry was predicted for each of the VPR conformers from the high-level molecular orbital calculations performed in the present study. It is well known that planar molecules generally have a small positive value of inertial defect due to the effect of zero-point vibrations. The inertial defects of the s-*trans*- and s-*cis*-VPRs are calculated from the experimentally determined rotational constants to be −0.072 and 0.018 uÅ^2, respectively. Although the negative value of the s-*trans*-VPR is inconsistent with the general behavior of planar molecules, the absolute value seems to be too small to conclude the molecular structure to be non-planar. The inertial defect calculated from the theoretically predicted rotational constants for the zero vibration level of the s-*trans*-VPR (*cf.* Table 1) also shows a negative value, −0.03 uÅ^2, so that the negative value of the s-*trans*-VPR is considered to be simply caused by the zero-point vibrations of the molecule. Effects of individual vibrational modes on the molecular rotational constants are seen from theoretically obtained vibration–rotation constant α summarized in Table S1 of the ESI.† However, it is difficult to specify particular vibrational modes causing the negative inertial defect, which is the sum result of the contributions of the 15 vibrational modes of the VPR.

The ground electronic state of the VPR is $\tilde{X}^2A''$, so that the unpaired electron is sitting in a molecular π-orbital consisting of the out-of-plane p-orbitals of the oxygen and carbon atoms. Following the McConnell relationship,[41,42] the Fermi coupling constant a_F of the protons of the VPR is predominantly proportional to the unpaired spin density on the carbon atom to which the proton is bonded. Due to the spin-polarization effect, a positive spin density on the carbon atom causes a negative spin density at the proton nucleus, resulting in a negative a_F value for the proton. As seen in Table 2, this is true for the –CH_2 protons of the VPR. The a_F values of all the –CH_2 protons of the VPR are almost constant, *ca.* − 10 MHz, and no conformer dependence is clearly seen. On the other hand, the signs of the a_F values of the –CH protons (H_3) are positive. This may be caused by a negative unpaired spin density[43] on the –CH carbon.

For halogen-substituted methyl radicals, CH_2F[44] and CH_2Cl,[45] which are typical carbon-centered π-radicals, each proton has a negative a_F value of *ca.* −60 MHz, which is 6 times as large as those of the –CH_2 protons of the VPR. Because *ca.* 85% unpaired electron density is estimated to be located on the carbon atom of the halogen-substituted methyl radicals,[45] about 10% unpaired electron density is expected on the –CH_2 carbon of the VPR. The VPR is generally considered as an oxygen-centered radical, described as structure 1 of Fig. 3.

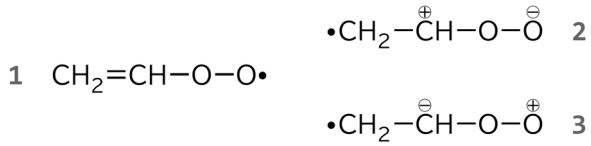

Fig. 3 Lewis structures of the vinylperoxy radical. (1) oxygen-centered radical. (2) and (3) carbon-centered radicals.

However, the experimental a_F values infer the non-negligible unpaired spin density on the –CH_2 carbon. Lewis structures with the unpaired electron located at the –CH_2 carbon can be depicted as structures 2 and 3 of Fig. 3, in which formal charges on the carbon and oxygen atoms are inverted to each other. Taking into account the electronegativities of carbon and oxygen, Lewis structure 2 seems to be the more appropriate formula. The zwitterionic character and the locations of the formal charges of structure 2 may reasonably explain the relatively large permanent dipole moments calculated for VPRs (*cf.* Table 1) and their directions (*cf.* Fig. 1). Furthermore, in Lewis structure 2, the –CH carbon has a vacant p-orbital, and the terminal oxygen has three lone pairs. If electrons of one of the three lone pairs are donated to the vacant p-orbital, a C–O bond may be formed between the –CH carbon and the terminal oxygen, resulting in the three-membered ring isomer, •CH_2-*c*-C(H)OO (dioxiranyl-methyl), which is postulated as an intermediate connecting the VPR to the HCHO + HCO dissociation channel, as mentioned in the Introduction section. The contribution of Lewis structure 2 may be an advantage for the formation of the three-membered ring intermediate from both of the two conformers.

The intensity of the FTMW spectrum observed for the VPR was much weaker than that expected from spectral intensity, for example, of CH_3OO[46] which is produced by a similar production scheme to the VPR, the association reaction of CH_3 + O_2, followed by collisional relaxation with third-body buffer gas atoms. It seems that collisional stabilization occurs only for a small portion of vibrationally excited nascent VPRs, and most of them might quickly dissociate either to the vinoxy radical + O or to formaldehyde + HCO under the present experimental conditions. For comparison of the spectral intensity of the VPR to those of the dissociation products, FTMW spectra of the vinoxy radical and formaldehyde were observed under the same experimental conditions as in the VPR observation. The observed spectra for the 2_{02}–1_{01} transition of the s-*trans*-VPR, the 1_{01}–0_{00} transition of the vinoxy radical, and the 2_{11}–2_{12} transition of formaldehyde are shown in Fig. 4 with the same intensity scale. The most intense fine/hyperfine components are present in the spectra of the s-*trans*-VPR and the vinoxy radical. Note that the intensity of the formaldehyde spectrum cannot be directly compared to those of the s-*trans*-VPR and the vinoxy radical, because the spectra of the radicals split into many fine and hyperfine components due to the unpaired electron and the three protons. However, it is obvious from Fig. 4 that the concentration of the vinoxy radical is higher than that of the s-*trans*-VPR in the jet expansion.

Taking into account the spectral intensity factors (thermal population, effect of fine/hyperfine splittings, and so on), relative concentrations of the three species in the jet expansion

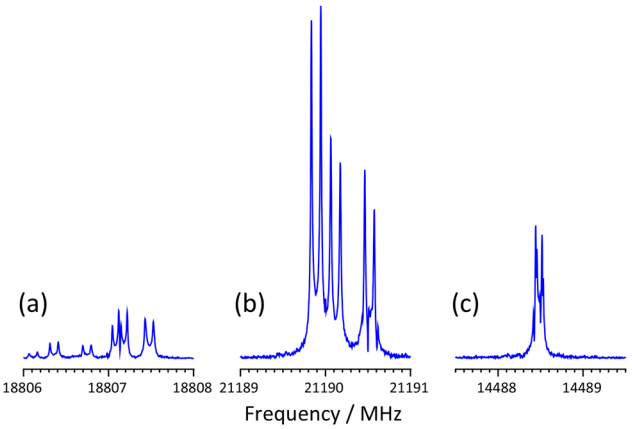

Fig. 4 FTMW spectra of (a) the 2_{02}–1_{01} transition of the s-*trans*-vinylperoxy radical, (b) the 1_{01}–0_{00} transition of the vinoxy radical, and (c) the 2_{11}–2_{12} transition of formaldehyde. The most intense fine/hyperfine components are involved in the spectra of the radicals. All the spectra were observed under the same discharged jet conditions, and are plotted with the same intensity scale. The spectrum of formaldehyde shows a very small splitting due to the nuclear spin angular momentum of the equivalent two protons (I_{total} = 1).

are roughly estimated from the spectral intensities of Fig. 4 to be 5 : 25 : 70 for the VPR, the vinoxy radical, and formaldehyde, respectively, by assuming a rotational temperature of 2.5 K. Detailed descriptions of this estimation are given in the ESI.† If the final product channels of the C_2H_3 + O_2 reaction are only three, yielding the stabilized VPR, the vinoxy radical, or formaldehyde, and all molecules of these three species were produced by this reaction in the present experiment, more than 90% of the association products (vibrationally excited VPRs) promptly proceed to the final product channels, CH_2CHO + O and HCHO + HCO. Only 5% of the association products are stabilized by collisions with the buffer gas even under the jet cooled conditions. Interestingly, Matsugi and Miyoshi[13] reported that the previously reported near-UV absorption of gas-phase VPR was absent in their experiment, although they conducted a similar experiment to the previous measurements.[24,27] They suggested that the previously reported spectra may be attributed to other transient species. There is no contradiction between the absence of the near-UV absorption and our estimation of the very small concentration of the gas-phase VPR. The branching fraction of the vinoxy radical + O channel has been experimentally determined to be *ca.* 20% by Oguchi *et al.*[12] under low pressure conditions. The experimentally determined fraction is reproduced by the theoretical calculation based on the RRKM theory.[13] The same calculation predicts the branching fraction of the formaldehyde + HCO channel to be slightly less than 80%. The present estimation of the relative concentrations of the three reaction products shows good agreement with the previous experimental and theoretical results of the reaction kinetic studies.

6. Conclusions

Pure rotational transitions of two conformers (s-*trans* and s-*cis*) of the vinylperoxy radical were observed by FTMW and FTWM–MW

double resonance spectroscopy. All the fine and hyperfine components observed in the FTMW spectra were fully assigned, and precise molecular parameters were determined for both conformers by least-squares analyses. Non-negligible unpaired electron density on the $-CH_2$ carbon was deduced from the experimentally determined Fermi coupling constants of the $-CH_2$ protons. The nature of the carbon-centered radical of the vinylperoxy radical reasonably explains the magnitudes and the directions of the theoretically calculated permanent dipole moments of the two conformers, and may work in favor of the isomerization to the intermediate with the three-membered ring structure finally leading to the HCHO + HCO product channel. The observed spectra of the vinylperoxy radical were weaker than expected. It is estimated that most of the nascent vinylperoxy radicals promptly dissociate to the final products, and less than 1/10 of them are collisionally stabilized and survive in the jet expansion.

Data availability

The data supporting this article have been included as part of the ESI.† The spectral data will be available from the authors upon request.

Conflicts of interest

There are no conflicts to declare.

Acknowledgements

The present study was supported by the Ministry of Science and Technology of Taiwan, MOST 104-2113-M-009-202. The authors thank Dr Keiichi Tanaka (Kyushu University) for kindly allowing us to use his stock of the precursor molecule, C_2H_3Br.

Notes and references

1 T. Carriere, P. Westmoreland, A. Kazakov, Y. Stein and F. Dryer, *Proc. Combust. Inst.*, 2002, **29**, 1257–1266.
2 J. G. Lopez, C. L. Rasmussen, M. U. Alzueta, Y. Gao, P. Marshall and P. Glarborg, *Proc. Combust. Inst.*, 2009, **32**, 367–375.
3 C. Xu and A. A. Konnov, *Energy*, 2012, **43**, 19–29.
4 M. Yang, Z. Wan, N. Tan, C. Zhang, J. Wang and X. Li, *Combust. Flame*, 2020, **221**, 20–40.
5 B. Su, M. Papp, I. Zsély, T. Nagy, P. Zhang and T. Turányi, *Combust. Flame*, 2024, **260**, 113201.
6 J.-Y. Park, M. C. Heaven and D. Gutman, *Chem. Phys. Lett.*, 1984, **104**, 469–474.
7 I. R. Slagle, J. Y. Park, M. C. Heaven and D. Gutman, *J. Am. Chem. Soc.*, 1984, **106**, 4356–4361.
8 A. Fahr and A. H. Laufer, *J. Phys. Chem.*, 1988, **92**, 7229–7232.
9 H. Krueger and E. Weitz, *J. Chem. Phys.*, 1988, **88**, 1608–1616.
10 V. D. Knyazev and I. R. Slagle, *J. Phys. Chem.*, 1995, **99**, 2247–2249.
11 A. J. Eskola and R. S. Timonen, *Phys. Chem. Chem. Phys.*, 2003, **5**, 2557–2561.
12 T. Oguchi, Y. Sato and H. Matsui, *Chem. Phys. Lett.*, 2009, **472**, 181–184.
13 A. Matsugi and A. Miyoshi, *Int. J. Chem. Kinet.*, 2014, **46**, 260–274.
14 B. K. Carpenter, *J. Am. Chem. Soc.*, 1993, **115**, 9806–9807.
15 B. K. Carpenter, *J. Phys. Chem.*, 1995, **99**, 9801–9810.
16 A. M. Mebel, E. W. G. Diau, M. C. Lin and K. Morokuma, *J. Am. Chem. Soc.*, 1996, **118**, 9759–9771.
17 R. Yang, L. Yu, X. Jin, M. Zhou and B. K. Carpenter, *J. Chem. Phys.*, 2005, **122**, 014511.
18 C. F. Goldsmith, L. B. Harding, Y. Georgievskii, J. A. Miller and S. J. Klippenstein, *J. Phys. Chem. A*, 2015, **119**, 7766–7779.
19 P. R. Westmoreland, *Combust. Sci. Technol.*, 1992, **82**, 151–168.
20 J. W. Bozzelli and A. M. Dean, *J. Phys. Chem.*, 1993, **97**, 4427–4441.
21 G. da Silva and J. W. Bozzelli, *J. Phys. Chem. A*, 2008, **112**, 3566–3575.
22 H. Wang, B. Wang, Y. He and F. Kong, *J. Chem. Phys.*, 2001, **115**, 1742–1746.
23 W. Feng and B. Wang, *Chem. Phys. Lett.*, 2002, **356**, 505–510.
24 H. Chishima, M. Koshi and K. Tonokura, *Chem. Lett.*, 2009, **38**, 1150–1151.
25 R. Mertens and C. von Sonntag, *Angew. Chem., Int. Ed. Engl.*, 1994, **33**, 1262–1264.
26 G. I. Khaikin and P. Neta, *J. Phys. Chem.*, 1995, **99**, 4549–4553.
27 A. Fahr, A. H. Laufer, M. Krauss and R. Osman, *J. Phys. Chem. A*, 1997, **101**, 4879–4886.
28 E. N. Sharp, PhD dissertation, The Ohio State University, Columbus, OH, 2008.
29 E. N. Sharp, P. Rupper and T. A. Miller, *Phys. Chem. Chem. Phys.*, 2008, **10**, 3955–3981.
30 H.-J. Werner, P. J. Knowles, G. Knizia, F. R. Manby, M. Schütz, P. Celani, W. Györffy, D. Kats, T. Korona, R. Lindh, A. Mitrushenkov, G. Rauhut, K. R. Shamasundar, T. B. Adler, R. D. Amos, S. J. Bennie, A. Bernhardsson, A. Berning, D. L. Cooper, M. J. O. Deegan, A. J. Dobbyn, F. Eckert, E. Goll, C. Hampel, A. Hesselmann, G. Hetzer, T. Hrenar, G. Jansen, C. Köppl, S. J. R. Lee, Y. Liu, A. W. Lloyd, Q. Ma, R. A. Mata, A. J. May, S. J. McNicholas, W. Meyer, T. F. Miller III, M. E. Mura, A. Nicklass, D. P. O'Neill, P. Palmieri, D. Peng, K. Pflüger, R. Pitzer, M. Reiher, T. Shiozaki, H. Stoll, A. J. Stone, R. Tarroni, T. Thorsteinsson, M. Wang and M. Welborn, *MOLPRO, version 2024.3, a package of ab initio programs*, 2024.
31 M. J. Frisch, G. W. Trucks, H. B. Schlegel, G. E. Scuseria, M. A. Robb, J. R. Cheeseman, G. Scalmani, V. Barone, G. A. Petersson, H. Nakatsuji, X. Li, M. Caricato, A. V. Marenich, J. Bloino, B. G. Janesko, R. Gomperts, B. Mennucci, H. P. Hratchian, J. V. Ortiz, A. F. Izmaylov, J. L. Sonnenberg, D. Williams-Young, F. Ding, F. Lipparini, F. Egidi, J. Goings, B. Peng, A. Petrone, T. Henderson, D. Ranasinghe, V. G. Zakrzewski, J. Gao, N. Rega, G. Zheng, W. Liang, M. Hada, M. Ehara, K. Toyota, R. Fukuda, J. Hasegawa, M. Ishida, T. Nakajima, Y. Honda, O. Kitao, H. Nakai, T. Vreven, K. Throssell, J. A. Montgomery, Jr., J. E. Peralta, F. Ogliaro, M. J. Bearpark, J. J. Heyd, E. N. Brothers, K. N. Kudin, V. N. Staroverov, T. A. Keith, R. Kobayashi, J. Normand, K. Raghavachari, A. P. Rendell, J. C. Burant, S. S. Iyengar,

J. Tomasi, M. Cossi, J. M. Millam, M. Klene, C. Adamo, R. Cammi, J. W. Ochterski, R. L. Martin, K. Morokuma, O. Farkas, J. B. Foresman and D. J. Fox, *Gaussian 16 Revision A.03*, Gaussian Inc., Wallingford CT, 2016.
32 S. L. Boyd, R. J. Boyd and L. R. C. Barclay, *J. Am. Chem. Soc.*, 1990, **112**, 5724–5730.
33 Y. Endo, H. Kohguchi and Y. Ohshima, *Faraday Discuss.*, 1994, **97**, 341–350.
34 T. J. Balle and W. H. Flygare, *Rev. Sci. Instrum.*, 1981, **52**, 33–45.
35 J.-U. Grabow and W. Stahl, *Z. Naturforsch., A: Phys. Sci.*, 1990, **45**, 1043–1044.
36 Y. Sumiyoshi, H. Katsunuma, K. Suma and Y. Endo, *J. Chem. Phys.*, 2005, **123**, 054324.
37 J. Brown and T. Sears, *J. Mol. Spectrosc.*, 1979, **75**, 111–133.
38 H. M. Pickett, *J. Mol. Spectrosc.*, 1991, **148**, 371–377.
39 **https://spec.jpl.nasa.gov/**.
40 M. Nakajima, Y.-T. Liu, C. H. Chang, K. Seiki, Y. Sumiyoshi, Y. Ohshima, J. Tang and Y. Endo, *Phys. Chem. Chem. Phys.*, 2022, **24**, 11585–11591.
41 H. M. McConnell, *J. Chem. Phys.*, 1956, **24**, 764–766.
42 H. M. McConnell and D. B. Chesnut, *J. Chem. Phys.*, 1958, **28**, 107–117.
43 H. M. McConnell and D. B. Chesnut, *J. Chem. Phys.*, 1957, **27**, 764–766.
44 Y. Endo, C. Yamada, S. Saito and E. Hirota, *J. Chem. Phys.*, 1983, **79**, 1605–1611.
45 Y. Endo, S. Saito and E. Hirota, *Can. J. Phys.*, 1984, **62**, 1347–1360.
46 K. Katoh, PhD dissertation, The University of Tokyo, Tokyo, 2007.

